Capacity Maximizing Adaptive Time-Switching Protocol for Energy Harvesting Full-Duplex Relaying Network over Rayleigh Fading Channel

Tan N. NGUYEN[1,*], *Peppino FAZIO*[2,3] *and Miroslav VOZNAK*[2]

[1]Communication and Signal Processing Research Group, Faculty of Electrical and Electronics Engineering, Ton Duc Thang University, Ho Chi Minh City, Vietnam
[2]Faculty of Electrical Engineering and Computer Science, Technical University of Ostrava, 70800 Ostrava, Czech Republic
[3]Department of Molecular Sciences and Nanosystems, Ca' Foscari University of Venice, Via Torino 155, 30123 Venezia VE, Italy

*Corresponding Author: Tan N. NGUYEN (email: nguyennhattan@tdtu.edu.vn)
(Received: 24-Jul-2022; accepted: 17-Oct-2022; published: 31-Dec-2022)
DOI: http://dx.doi.org/10.55579/jaec.202264.386

Abstract. *This paper studies a decode-and-forward (DF) full-duplex cooperative relaying network, whereas one transmitter S transmits information to one receiver D via the help of a relay R. In particular, the transmitter can simultaneously transmit energy and information (SWIPT) to relay R using time-switching (TS) method. Then, relay R can utilize the harvested energy to transfer information to the receiver D. Based on the proposed system model, we derive the mathematical expressions for the system capacity for the proposed non-adaptive TS (NATSP) and adaptive TS protocols (ATSP). Next, the Monte Carlo simulations are executed to corroborate the exactness of the analysis compared to the numerical results. Both numerical and analytical results show the superiority of ATSP over NATSP.*

Keywords

Capacity, Energy harvesting, Full duplex, Rayleigh fading, Time switching.

1. Introduction

Recently, the Internet of things (IoT) has received great attention from both industrial and academic because of its important role in the fifth generation (5G) and beyond [1–6]. The work in [1] investigated the performance of the cognitive IoTs networks by employing multiple relays via a deep learning approach. It, however, focuses on outage probability rather than the ergodic capacity. Authors in [2] also applied artificial intelligence (AI) to address the security issue in energy harvesting-enabled IoT networks. The backscatter-assisted mobile edge computing in IoTs networks was studied in [3]. Particularly, by optimizing the transmit power at the gateway, the time-switching ratio of the sum rate is maximized. Liu and others in [4] also maximized the transmission rate under the constraint of total transmit power and resource allocations. These works, however, rely on the numerical approach to obtain the optimal solution rather than based on the rigorous mathematical framework. On the other hand, resource allocation in the unmanned aerial vehicle (UAV)

was investigated in [6]. Nonetheless, they do not take into account energy harvested at UAV.

Besides the great benefits of IoT, the enormous number of IoT devices imposes many challenges in communications due to limitations of resources, i.e., available frequency. Owing to the development of self-interference cancellation (SIC) techniques that can obtain a high SI cancelation, full-duplex (FD) is a potential technique to improve the spectrum efficiency by its capability of transmitting and receiving signals at the same time [7, 8]. Due to the above-mentioned advantages, FD has been widely investigated in cooperative relay networks [9–11].

Besides the restriction on the spectrum, IoT devices are usually equipped with limited energy capacity. Battery replacement/recharging is not always convenient or even impossible. Furthermore, the significant increase in resource-intensive IoT applications such as augmented reality (AR), multi-view video construction, and reality (VR) puts more demands on energy consumption and can significantly reduce equipment's lifetime. Thanks to the development of energy harvesting (EH) techniques, it can become a promising solution to overcome the energy problem of IoT devices. Especially, radio frequency (RF) EH has received great interest due to its controllability and predictability as compared with other ambient resources such as wind [12, 13], solar [14], or water [15]. Consequently, RF EH has been intensively investigated in cooperative relay communications [16–18]. Indeed, RF EH can be divided into two types, termed wireless power transfer (WPT) [16–18] and simultaneous wireless information and power transfer (SWIPT). The main difference between WPT and SWIPT is that the RF signal only carries energy in WPT while it can contain both energy and information in the SWIPT technique.

Motivated by the above discussions, this paper studied the system capacity analysis of a SWIPT- and FD-assisted cooperative relay network. Besides, the relay node is equipped with an EH circuit, and it can harvest energy from a transmitter's RF signals. The contributions of this paper are summarized as follows:

- We investigated and proposed a SWIPT- and FD-aided relay network with one transmitter, one FD relay, and one receiver.
- By considering the above system model, we proposed two protocols, namely, non-adaptive time-switching (NATSP) and adaptive time-switching protocols (ATSP). Besides, we derive the mathematical expression for the system capacity corresponding to each protocol.
- Then, the mathematical results are confirmed through Monte Carlo simulations.

This paper is organized as follows. In Section 2, the system model of the SWIPT- and FD-assisted relay network is described in detail. Then, the system capacity is analyzed in Section 3. The simulation results to validate our analysis are presented in Section 4. Finally, Section 5 concludes the paper.

2. System Model

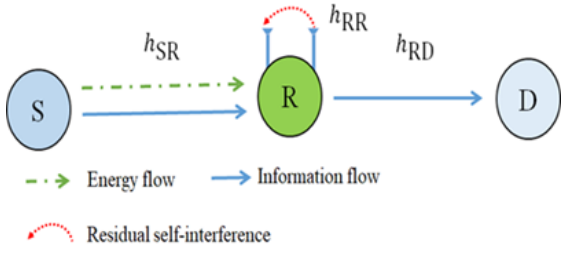

Fig. 1: System model.

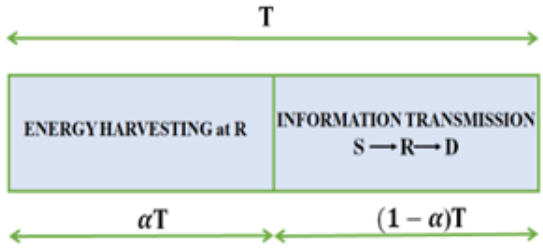

Fig. 2: Energy Harvesting and Information transmission processing.

As shown in Fig. 1, a transmitter S can transmit both information and energy to a relay R. Moreover, relay R is equipped with an energy harvester circuit, and it can harvest energy from the transmitter's RF signals. The transmitter S and receiver D operate at half-duplex mode, while relay R can operate at full-duplex mode. The energy harvesting and information transmission of our system are presented in Fig. 2. More specifically, relay R harvests energy during the first time slot αT and transmits data to receiver D during the second time slot $(1-\alpha)T$. The channels between any two users are assumed to follow block Rayleigh fading. Thus, the squared amplitudes of the channel gains such as $|h_{SR}|^2, |h_{RR}|^2$, etc. are exponential random variables (RVs) whose cumulative distribution function (CDF) and probability density function (PDF) have the following forms, respectively:

$$F_{|h_i|^2}(x) = 1 - \exp\left(-\lambda_i x\right), \tag{1}$$

$$f_{|h_i|^2}(x) = \lambda_i \exp\left(-\lambda_i x\right). \tag{2}$$

where $i \in (SR, RD, RR)$ and λ_i is the mean of random variables (RVs) $|h_i|^2$, respectively.

From Fig. 1, the received signal at the relay can be expressed by

$$y_R = h_{SR}x_s + h_{RR}x_R + n_R, \tag{3}$$

where x_S is the S's signal with $\mathrm{E}\left\{|x_s|^2\right\} = P_s$; x_R is the self-interference at R due to full-duplex relaying and satisfies $\mathrm{E}\left\{|x_R|^2\right\} = P_R$, where $\mathrm{E}\{\bullet\}$ denotes the expectation operation; n_R is the additive white Gaussian noise (AWGN) at R. The harvested energy at R during the first time slot can be computed by

$$E_R = \eta\alpha T P_s |h_{SR}|^2, \tag{4}$$

By applying the time-switching (TS) scheme, the average transmit power at R can be thus obtained as [19]

$$P_R = \frac{E_R}{(1-\alpha)T} = \frac{\eta\alpha P_s |h_{SR}|^2}{(1-\alpha)} = \mu P_s |h_{SR}|^2, \tag{5}$$

where $0 < \eta \leq 1$ is the energy conversion efficiency and $\mu \triangleq \eta\alpha/(1-\alpha)$.

Because relay R can perform full-duplex mode, the signal to interference noise (SINR) at the relay R can be given by

$$\gamma_R = \frac{P_s |h_{SR}|^2}{|h_{RR}|^2 P_R + N_0}. \tag{6}$$

By substituting (5) into (6) and assuming that $N_0 << P_S|h_{\mathrm{RR}}|^2$, then we have

$$\gamma_R = \frac{P_s |h_{SR}|^2}{\mu P_s |h_{SR}|^2 |h_{RR}|^2 + N_0} \approx \frac{1}{\mu |h_{RR}|^2}. \tag{7}$$

Next, the received signal and SNR at D in the second time slot can be respectively given by

$$y_D = h_{RD}x_R + n_D, \tag{8}$$

$$\gamma_D = \frac{P_R |h_{RD}|^2}{N_0} = \mu\Psi |h_{SR}|^2 |h_{RD}|^2, \tag{9}$$

where $\Psi = \frac{P_S}{N_0}$ and n_D is the zero mean AWGN with variance N_0.

Because we use the decode-and-forward (DF) protocol in our system model. Therefore, the end-to-end SNR and the total received capacity at D can be expressed as, respectively

$$\gamma_{DF} = \min\left(\gamma_R, \gamma_D\right), \tag{10}$$

$$C_{DF} = \log_2\left(1 + \gamma_{DF}\right). \tag{11}$$

3. Performance Analysis

3.1. Case 1: Non-adaptive time-switching protocol (NATSP)

The communication capacity of the system can be expressed as [20]

$$C_{DF} = \frac{1}{\ln 2} \int_0^\infty \frac{1 - F_{\gamma_{DF}}(x)}{1+x} dx, \tag{12}$$

From (12), the CDF of γ_{DF} is given by

$$\begin{aligned} F_{\gamma_{DF}}(x) &= \Pr\left(\gamma_{DF} < x\right) \\ &= \Pr\left(\min\left(\gamma_R, \gamma_D\right) < x\right), \end{aligned} \tag{13}$$

By substituting (7) and (9) into (13), $F_{\gamma_{DF}}$ can be reformulated as

$$\begin{aligned} F_{\gamma_{DF}}(x) &= \Pr\left(\min\left(\frac{1}{\mu|h_{\mathrm{RR}}|^2}, \mu\Psi|h_{\mathrm{SR}}|^2|h_{\mathrm{RD}}|^2\right) < x\right) \\ &= 1 - \underbrace{\Pr\left(\frac{1}{\mu|h_{\mathrm{RR}}|^2} \geq x\right)}_{P_1} \\ &\times \underbrace{\Pr\left(\mu\Psi|h_{\mathrm{SR}}|^2|h_{\mathrm{RD}}|^2 \geq x\right)}_{P_2}, \end{aligned} \tag{14}$$

First, P_1 in (14) can be calculated by

$$\begin{aligned} P_1 &= \Pr\left(\frac{1}{\mu|h_{RR}|^2} \geq x\right) \\ &= \Pr\left(|h_{RR}|^2 \leq \frac{1}{\mu x}\right) = 1 - \exp\left(-\frac{\lambda_{RR}}{\mu x}\right), \end{aligned} \tag{15}$$

Second, P_2 in (14) can be computed as

$$\begin{aligned} P_2 &= \Pr\left(\mu\Psi|h_{SR}|^2|h_{RD}|^2 \geq x\right) \\ &= 1 - \Pr\left(|h_{SR}|^2 < \frac{x}{\mu\Psi|h_{RD}|^2}\right) \\ &= 1 - \int_0^\infty F_{|h_{SR}|^2}\left(\frac{x}{\mu\Psi y}\right) \times f_{|h_{RD}|^2}(y)dy \\ &= \int_0^\infty \lambda_{RD} \exp\left(-\frac{x\lambda_{SR}}{\mu\Psi y} - \lambda_{RD}y\right), \end{aligned} \tag{16}$$

By using [21, Eq. 3.324.1], (16) can be rewritten by

$$P_2 = 2\sqrt{\frac{x\lambda_{SR}\lambda_{RD}}{\mu\Psi}} \times K_1\left(2\sqrt{\frac{x\lambda_{SR}\lambda_{RD}}{\mu\Psi}}\right), \tag{17}$$

where $K_v(\bullet)$ is the modified Bessel function of the second kind and v-th order.

By substituting (15), (17) into (13), and then into (12), the system capacity can be obtained in the next top of page.

3.2. Case 2: Adaptive time-switching protocol (ATSP)

In this case, we optimize the time-switching ratio α^* to maximize the capacity of our proposed system. Because the DF protocol is considered in our work, the α^* can be obtained by solving the following equation

$$\begin{aligned} &\gamma_R = \gamma_D \leftrightarrow \frac{1}{\mu|h_{RR}|^2} = \mu\Psi|h_{SR}|^2|h_{RD}|^2 \\ &\rightarrow \mu^2 = \frac{1}{|h_{RR}|^2|h_{SR}|^2|h_{RD}|^2\Psi} \\ &\rightarrow \alpha^* = \frac{1}{\eta\sqrt{|h_{RR}|^2|h_{SR}|^2|h_{RD}|^2\Psi}+1}. \end{aligned} \tag{19}$$

By substituting (19) into (13), the $F^*_{\gamma_{DF}}$ can be thus expressed by

$$\begin{aligned} F^*_{\gamma_{DF}}(x) &= \Pr\left(\frac{\sqrt{|h_{RR}|^2|h_{SR}|^2|h_{RD}|^2\Psi}}{|h_{RR}|^2} < x\right) \\ &= \Pr\left(\frac{|h_{SR}|^2|h_{RD}|^2\Psi}{|h_{RR}|^2} < x^2\right) \\ &= \Pr\left(|h_{SR}|^2|h_{RD}|^2 < \frac{x^2|h_{RR}|^2}{\Psi}\right) \\ &= \int_0^\infty F_X\left(\frac{x^2y}{\Psi}\right) \times f_{|h_{RR}|^2}(y)dy. \end{aligned} \tag{20}$$

where $X = |h_{SR}|^2|h_{RD}|^2$.

By applying (17), equation (20) can be reformulated at the next top of the page.

Let us denote $t = \sqrt{y}$, (21) can be rewritten at the next top of the page.

With the help of [21, Eq. 3.324.1], $F^*_{\gamma_{DF}}$ can be given by

$$F^*_{\gamma_{DF}}(x) = 1 - \exp\left(\frac{x^2\lambda_{SR}\lambda_{RD}}{2\Psi\lambda_{RR}}\right) W_{-1,\frac{1}{2}}\left(\frac{x^2\lambda_{SR}\lambda_{RD}}{\Psi\lambda_{RR}}\right), \tag{23}$$

where $W(\bullet)$ is the Whittaker function.

Finally, the system capacity can be mathematically expressed as

$$C^*_{DF} = \frac{1}{\ln 2}\int_0^\infty \frac{\exp\left(\frac{x^2\lambda_{SR}\lambda_{RD}}{2\Psi\lambda_{RR}}\right) W_{-1,\frac{1}{2}}\left(\frac{x^2\lambda_{SR}\lambda_{RD}}{\Psi\lambda_{RR}}\right)}{1+x}dx. \tag{24}$$

4. Numerical Results

In this section, we provide the numerical results to corroborate the accuracy of the analysis, i.e., the system capacity. More specifically, the results can be obtained by averaging 10^6 channel

$$C_{DF} = \frac{2}{\ln 2} \int_0^{\infty} \frac{\left(1 - \exp\left(-\frac{\lambda_{RR}}{\mu\gamma_{th}}\right)\right) \times \sqrt{\frac{x\lambda_{SR}\lambda_{RD}}{\mu\Psi}} \times K_1\left(2\sqrt{\frac{x\lambda_{SR}\lambda_{RD}}{\mu\Psi}}\right)}{1+x} dx. \tag{18}$$

$$F^*_{\gamma_{DF}}(x) = 1 - 2\int_0^{\infty} \lambda_{RR} \exp\left(-\lambda_{RR} y\right) \sqrt{\frac{x^2 y \lambda_{SR}\lambda_{RD}}{\Psi}} K_1\left(2\sqrt{\frac{x^2 y \lambda_{SR}\lambda_{RD}}{\Psi}}\right) dy. \tag{21}$$

$$F^*_{\gamma_{DF}}(x) = 1 - 4x\lambda_{RR}\sqrt{\frac{\lambda_{SR}\lambda_{RD}}{\Psi}} \int_0^{\infty} t^2 \exp\left(-\lambda_{RR} t^2\right) K_1\left(2xt\sqrt{\frac{\lambda_{SR}\lambda_{RD}}{\Psi}}\right) dt, \tag{22}$$

Tab. 1: Simulation parameters.

Symbol	Parameter name	Fixed value	Varying range
η	energy conversion efficiency	0.8	0.05 to 1
α	time switching factor	0.25, 0.355, 0.55, 0.75	0.05 to 0.95
λ_{SR}	Parameter of channel power gain $\lvert h_{\mathrm{SR}}\rvert^2$	1	0.5 to 4
λ_{RD}	Parameter of channel power gain of $\lvert h_{\mathrm{RD}}\rvert^2$	1	0.5 to 4
λ_{RR}	Parameter of SI channel power gain of $\lvert h_{\mathrm{RR}}\rvert^2$	1	0.5 to 4
Ψ	Transmit power-to-noise-ratio from source	3 dB	-5 to 15 dB

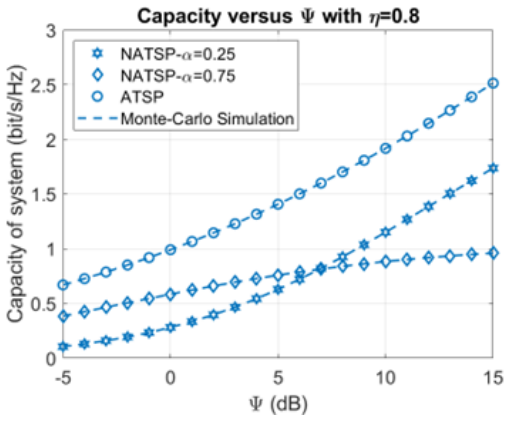

Fig. 3: Capacity versus Ψ (dB) with $\eta = 0.8$.

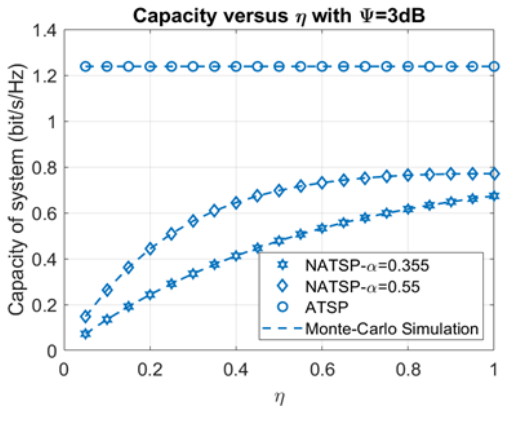

Fig. 4: Capacity versus η with $\Psi = 3(dB)$.

realizations [22–24]. The simulation parameters are listed in Tab. 1.

In Figs. 3 and 4, we sketch the system capacity as a function of Ψ(dB) with $\eta = 0.8$ and different α values. It can be observed from Fig. 3 that the larger the Ψ value is, the better the system capacity can be acquired. Moreover, the system capacity is proportional to the Ψ value. It is expected because if we allocate more transmit power to transmitter S, the data transmission rate at receiver D is significantly improved. In particular, when Ψ<7 dB, the system capacity of the NATSP scheme with $\alpha = 0.25$ outperforms the NATSP scheme with $\alpha = 0.75$. Nevertheless, when Ψ>7 dB, the NATSP scheme performance is worse than the NATSP scheme with $\alpha = 0.75$. Moreover, the ATSP performance is always better than that compared to others because it does not depend on α value and it is designed by maximizing the end-to-end SNR at D.

Figure 4 shows the system capacity as a function of energy conversion efficiency η, where Ψ=3 dB. As can be observed from Fig. 4 that the system performance of the NATSP is greatly increased with the higher value of η. In addition, the NATSP scheme with α=0.355 can obtain a better capacity compared to the NATSP scheme with $\alpha = 0.55$. Especially, the system capacity of the ATSP scheme is unchanged. It can be explained based on (24) in which the capacity expression does not depend on η value.

In Fig. 5, we investigate the effects of the time-switching factor α on the system capacity, with $\eta = 0.8$. The time-switching ratio is crucial because it affects both the time allocation for energy harvesting and information transmission. It can be observed that the system capacity of the NATSP is greatly enhanced when α increases to an optimal point, then it becomes worse. It is because the higher the α value is, the more the allocation time is used for energy harvesting, and less time is used for information transmission. Therefore, there exists an optimal point of α to maximize the system capacity. Similar to Fig. 4, the ATSP obtains a better performance compared to NATSP. However, the capacity of ATSP is unaltered with increasing of α. Furthermore, the system capacity is significantly increased when Ψ is from 1 dB to 4 dB.

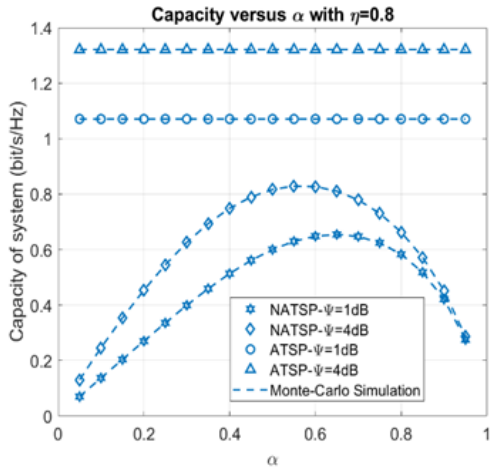

Fig. 5: Capacity versus α with $\eta = 0.8$.

Figure 6 plots the system capacity as a function of $\lambda_{\mathrm{SR}} = \lambda_{\mathrm{RD}}$, where $\eta = 0.8, \Psi = 3\mathrm{dB}, \mathrm{and}\lambda_{\mathrm{RR}} = 1$.Moreover, the parameter λ_i with $i \in \{\mathrm{SR}, \mathrm{RR}, \mathrm{RD}\}$ can be defined as $\lambda_i = (d_i)^{\beta}$, where β is the path loss exponent. Therefore, $\lambda_{\mathrm{SR}} = \lambda_{\mathrm{RD}}$ implies that the distance between S $\rightarrow$ R equals to the distance between R $\rightarrow$ D.It can be seen from Fig. 6 that the system capacity is significantly decreased with a larger distance from source/relay to relay/destination. It can be explained by the fact that the larger the distance is, the more channel attenuation can be obtained. Therefore, it reduces the channel quality, which deteriorates the system's capacity.

In Fig. 7, the impact of self-interference (SI) level, which represents by the channel parameter λ_{RR}, on the capacity performance is studied. In this simulation, it is worth noting that higher λ_{RR} corresponds to a lower SI level, i.e. better SI cancellation solution due to $1/\lambda_{\mathrm{RR}}$ is the mean of SI channel power gain $|h_{\mathrm{RR}}|^2$. It can be observed that when the SI level is increased, the capacity is decreased. This can be explained that based on the definition of capacity in equation (12), when the SI level is reduced, $1 - F_{\gamma_{\mathrm{DF}}}(x)$ will be increased, hence the capacity will be also increased.

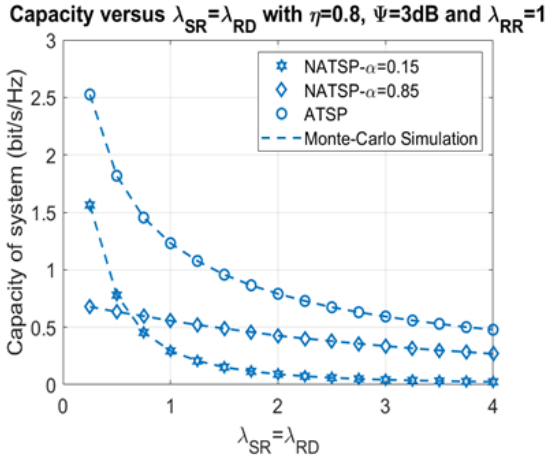

Fig. 6: Capacity versus λ with η=0.8, Ψ = 3 dB and $\lambda_{RR} = 1$.

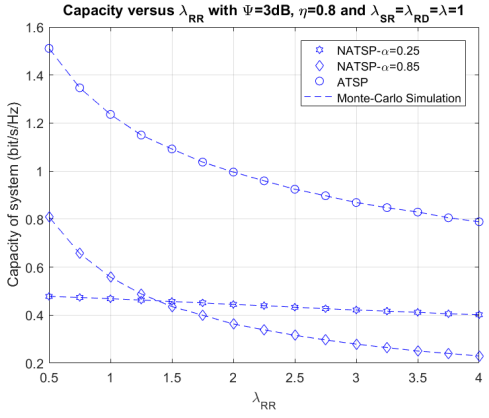

Fig. 7: Capacity versus λ_{RR} with λ_{SR}=λ_{RD}=λ=1, η = 0.8 and Ψ = 3 dB.

5. Conclusions

This paper studied a cooperative relay network with a transmitter S, a relay R, and a receiver D. Further, the relay user can harvest energy from a transmitter S and use harvested energy to transmit information to D. In particular, the transmitter S can transmit both information and energy to R simultaneously (SWIPT) applying time-switching method. In this context, we derive the system capacity at the receiver for both non-adaptive time-switching (NATSP) and adaptive time-switching protocols (ATSP). The numerical results are presented to validate the correctness of our analysis. The results show the superiority of our proposed ATSP compared to NATSP. The results obtained from this work can motivate interesting future work such as a more generalized model, i.e., Rician or Nakagami-m fading channels.

Acknowledgement

This research was supported by the Ministry of Education, Youth and Sports of the Czech Republic under the grant SP2021/25 and e-INFRA CZ (ID:90140).

References

[1] Nguyen, T.V., Tran, T.N., Shim, K., Huynh-The, T., & An, B. (2021). A Deep-Neural-Network-Based Relay Selection Scheme in Wireless-Powered Cognitive IoT Networks. *IEEE Internet of Things Journal*, *8*(9), 7423–7436.

[2] Mao, B., Kawamoto, Y., & Kato, N. (2020). AI-Based Joint Optimization of QoS and Security for 6G Energy Harvesting Internet of Things. *IEEE Internet of Things Journal*, *7*(8), 7032–7042.

[3] Nguyen, P.X., Tran, D.H., Onireti, O., Tin, P.T., Nguyen, S.Q., Chatzinotas, S., & Vincent Poor, H. (2021). Backscatter-Assisted Data Offloading in OFDMA-Based Wireless-Powered Mobile Edge Computing for IoT Networks. *IEEE Internet of Things Journal*, *8*(11), 9233–9243.

[4] Liu, X. & Zhang, X. (2019). Rate and Energy Efficiency Improvements for 5G-Based IoT With Simultaneous Transfer. *IEEE Internet of Things Journal*, *6*(4), 5971–5980.

[5] Moudoud, H., Khoukhi, L., & Cherkaoui, S. (2021). Prediction and Detection of FDIA and DDoS Attacks in 5G Enabled IoT. *IEEE Network*, *35*(2), 194–201.

[6] Tran, D.H., Nguyen, V.D., Gautam, S., Chatzinotas, S., Vu, T.X., & Ottersten, B.

(2020). Resource Allocation for UAV Relay-Assisted IoT Communication Networks. In *2020 IEEE Globecom Workshops (GC Wkshps*, 1–7.

[7] Nguyen, T.N., Tran, D.H., Phan, V.D., Voznak, M., Chatzinotas, S., Ottersten, B., & Poor, H.V. (2022). Throughput Enhancement in FD- and SWIPT-Enabled IoT Networks Over Nonidentical Rayleigh Fading Channels. *IEEE Internet of Things Journal*, *9*(12), 10172–10186.

[8] Huang, H., Hu, S., Yang, T., & Yuan, C. (2021). Full-Duplex Nonorthogonal Multiple Access With Layers-Based Optimized Mobile Relays Subsets Algorithm in B5G/6G Ubiquitous Networks. *IEEE Internet of Things Journal*, *8*(20), 15081–15095.

[9] Ba, C.N., Tran, M.H., Tran, P.T., & Nguyen, T.N. (2020). Outage probability of NOMA system with wireless power transfer at source and full-duplex relay. *AEU - International Journal of Electronics and Communications*, *116*, 152957.

[10] Nguyen, T.N., Tran, M., Nguyen, T.L., & Voznak, M. (2019). Adaptive relaying protocol for decode and forward full-duplex system over Rician fading channel: System performance analysis. *China Communications*, *16*(3), 92–102.

[11] Zhu, L., Zhang, J., Xiao, Z., Cao, X., Xia, X.G., & Schober, R. (2020). Millimeter-Wave Full-Duplex UAV Relay: Joint Positioning, Beamforming, and Power Control. *IEEE Journal on Selected Areas in Communications*, *38*, 2057–2073.

[12] Kong, F., Dong, C., Liu, X., & Zeng, H. (2014). Quantity Versus Quality: Optimal Harvesting Wind Power for the Smart Grid. *Proceedings of the IEEE*, *102*(11), 1762–1776.

[13] Zhao, L., Tang, L., Liang, J., & Yang, Y. (2017). Synergy of Wind Energy Harvesting and Synchronized Switch Harvesting Interface Circuit. *IEEE/ASME Transactions on Mechatronics*, *22*(2), 1093–1103.

[14] Hieu, T.D., Dung, L.T., & Kim, B.S. (2016). Stability-Aware Geographic Routing in Energy Harvesting Wireless Sensor Networks. *Sensors*, *16*(5).

[15] Fooladivanda, D., Domínguez-García, A.D., & Sauer, P.W. (2019). Utilization of Water Supply Networks for Harvesting Renewable Energy. *IEEE Transactions on Control of Network Systems*, *6*(2), 763–774.

[16] Tin, P.T., Dinh, B.H., Nguyen, T.N., Ha, D.H., & Trang, T.T. (2020). Power Beacon-Assisted Energy Harvesting Wireless Physical Layer Cooperative Relaying Networks: Performance Analysis. *Symmetry*, *12*(1).

[17] Wu, Q., Zhang, G., Ng, D.W.K., Chen, W., & Schober, R. (2019). Generalized Wireless-Powered Communications: When to Activate Wireless Power Transfer? *IEEE Transactions on Vehicular Technology*, *68*(8), 8243–8248.

[18] Hieu, T.D., Duy, T.T., & Kim, B.S. (2018). Performance Enhancement for Multihop Harvest-to-Transmit WSNs With Path-Selection Methods in Presence of Eavesdroppers and Hardware Noises. *IEEE Sensors Journal*, *18*(12), 5173–5186.

[19] Voznak, M., Tran, H.Q.M., & Nguyen, N.T. (2018). The System Performance of Half-Duplex Relay Network under Effect of Interference Noise. *Journal of Advanced Engineering and Computation*, *2*(1).

[20] Tin, P.T., Nguyen, T.N., Tran, M., Trang, T.T., & Sevcik, L. (2020). Exploiting Direct Link in Two-Way Half-Duplex Sensor Network over Block Rayleigh Fading Channel: Upper Bound Ergodic Capacity and Exact SER Analysis. *Sensors*, *20*(4).

[21] Gradshteyn, I.S. & Ryzhik, I.M. (2014). *Table of integrals, series, and products*. Academic press.

[22] Nguyen, T.N., Quang Minh, T.H., Tran, P.T., & Vozňák, M. (2018). Energy Harvesting over Rician Fading Channel: A Performance Analysis for Half-Duplex Bidirectional Sensor Networks under Hardware Impairments. *Sensors*, *18*(6).

[23] Nguyen, T.N., Tu, L.T., Tran, D.H., Phan, V.D., Voznak, M., Chatzinotas, S., & Ding, Z. (2022). Outage Performance of Satellite Terrestrial Full-Duplex Relaying Networks With co-Channel Interference. *IEEE Wireless Communications Letters*, *11*(7), 1478–1482.

[24] Nguyen, T.N., Duy, T.T., Tran, P.T., Voznak, M., Li, X., & Poor, H.V. (2022). Partial and Full Relay Selection Algorithms for AF Multi-Relay Full-Duplex Networks With Self-Energy Recycling in Non-Identically Distributed Fading Channels. *IEEE Transactions on Vehicular Technology*, *71*(6), 6173–6188.

About Authors

Tan N. NGUYEN was born in Nha Trang City, Vietnam, in 1986. He received B.S. and M.S. degrees in electronics and telecommunications engineering from Ho Chi Minh University of Natural Sciences, and member of Vietnam National University at Ho Chi Minh City (Vietnam) in 2008 and 2012, respectively. He is currently pursuing his Ph.D. degree in electrical engineering at VSB Technical University of Ostrava, Czech Republic. He got his Ph.D. degree in computer science, communication technology, and applied mathematics at VSB-Technical University of Ostrava, Czech Republic, in 2019. In 2013, he joined the Faculty of Electrical and Electronics Engineering of Ton Duc Thang University, Vietnam, and has been working as a lecturer since then. His major interests are cooperative communications, cognitive radio, signal processing, and physical layer security.

Peppino FAZIO was born in Catanzaro in 1977 and took master's degree in Computer Engineering in 2004 at University of Calabria (UNICAL) with his thesis named "A New Algorithm of Rate Adaptation and Call Admission Control for QoS Optimization in Wireless Networks with a Slow Fading Channel". At the end of 2004, he started my Ph.D. activity in Electronics and Communications Engineering at UNICAL on mobility prediction, channel modeling, resource reservation and vehicular communications. He took my Ph.D. in 2008 with his thesis titled "Resource Reservation Protocol and Predictive Algorithms for QoS support in Wireless Environments". In the middle of 2008, he has been at the "Universidad Politecnica" of Valencia (UPV) for several months, in order to make some post-doc research on vehicular networks and, in particular, the multi-channel structure of MAC in VANETs. His research interests include also mobile communication networks, QoS architectures, and internetworking.

Miroslav VOZNAK received his Ph.D. in telecommunications in 2002 from the Faculty of Electrical Engineering and Computer Science at VSB – Technical University of Ostrava and achieved habilitation in 2009. He was appointed Full Professor in Electronics and Communications Technologies in 2017. His research interests generally focus on ICT, especially on the quality of service and experience, network security, wireless networks, and big data analytics. He has authored and co-authored over one hundred articles indexed in SCI/SCIE journals. According to the Stanford University study released in 2020, he is one of the World's Top 2% of scientists in Networking & Telecommunications, and Information & Communications Technologies. He served as a general chair of the 11th IFIP Wireless and Mobile Networking Conference in 2018 and the 24th IEEE/ACM International Symposium on Distributed Simulation and Real-Time Applications in 2020. He participated in six projects funded by EU in programs managed directly by European Commission. Currently, he is a principal investigator in the research project QUANTUM5 funded by NATO, which focuses on the application of quantum cryptography in 5G campus networks.